J. Fluid Mech. (2012), *vol.* 709, *pp.* 610–621. © Cambridge University Press 2012
doi:10.1017/jfm.2012.355

On flow in weakly precessing cylinders: the general asymptotic solution

Xinhao Liao[1] **and Keke Zhang**[2]†

[1] Shanghai Astronomical Observatory, Chinese Academy of Sciences, Shanghai 200030, China
[2] Department of Mathematical Sciences, University of Exeter, Exeter EX4 4QE, UK

(Received 9 April 2012; revised 18 April 2012; accepted 5 July 2012;
first published online 24 August 2012)

We investigate, through both asymptotic and numerical analysis, precessionally driven flow of a homogeneous fluid confined in a fluid-filled circular cylinder that rotates rapidly about its symmetry axis and precesses slowly about a different axis that is fixed in space. After demonstrating that the inviscid approximation is always divergent even far away from resonance, we derive a general asymptotic solution for an asymptotically small Ekman number in the rotating frame of reference describing the weakly precessing flow that satisfies the no-slip boundary condition and that is valid at or near or away from resonance. Numerical analysis of the same problem using the Galerkin method in terms of a Chebyshev polynomial expansion is also carried out, showing satisfactory agreement between the general asymptotic solution and the corresponding numerical solution at or near or away from resonance.

Key words: boundary layer structure, rotating flows, waves in rotating fluids

1. Introduction

Motivated by the wish to understand the stability properties of spinning spacecraft with fluid payloads as well as the key dynamics of planetary precession, considerable attention has been paid to the problem of fluid motion in a precessing cylinder (for example, Wood 1966; Gans 1970; Manasseh 1992; Kobine 1995; Meunier *et al.* 2008). The problem is concerned with a homogeneous fluid of viscosity ν confined in a fluid-filled circular cylinder of height d and radius Γd that rotates rapidly with angular velocity $\boldsymbol{\Omega}_0$ about its symmetry axis and precesses slowly with angular velocity $\boldsymbol{\Omega}_p$ about a different axis that is fixed in space. Three key dimensionless parameters characterize the problem: the Ekman number $Ek = \nu/|\boldsymbol{\Omega}_0|d^2$ providing the measure of relative importance between the typical viscous force and the Coriolis force (Greenspan 1968), the Poincaré number $Po = |\boldsymbol{\Omega}_p|/|\boldsymbol{\Omega}_0|$ quantifying the strength of the precessional forcing (Wu & Roberts 2009) and the radius–height aspect ratio Γ controlling the condition of resonance (Gans 1970).

Under the assumption that the solution of weakly precessing flow ($Po \ll 1$ and $(Po/\sqrt{Ek}) \ll 1$) at resonance can be approximated by a single inertial mode, Gans (1970) showed that the primary resonances take place at the aspect ratios $\Gamma = 0.502559$ or $\Gamma = 1.045945$ or $\Gamma = 1.611089$, where the frequency of the Poincaré force is the same as that of the primary inertial mode and the amplitude $|\boldsymbol{u}|$

† Email address for correspondence: kzhang@ex.ac.uk

https://doi.org/10.1017/jfm.2012.355 Published online by Cambridge University Press

of the flow obeys the asymptotic scaling $|\boldsymbol{u}| = O(Po/\sqrt{Ek})$ at $Ek \ll 1$. Meunier *et al.* (2008) extended the analysis of Gans (1970) by deriving the weakly nonlinear amplitude equations for the primary resonances under the assumption that the precessing flow is still dominated by a single resonant inertial mode that is coupled with the geostrophic mode when nonlinearity becomes sufficiently strong. When far away from the primary resonances, an inviscid solution at $Ek = 0$, based on the expansion of inertial modes neglecting the viscous effect, was also derived (for example, Wood 1966; Manasseh 1992), revealing that the amplitude of the non-resonant flow obeys the scaling $|\boldsymbol{u}| = O(Po)$. It was thought that the inviscid solution would offer a true approximation to the precessing flow in the weaker forcing regimes far away from resonance. Experimentally, Manasseh (1992) demonstrated that the strongly precessing flow at resonance exhibits a rich dynamics, including transition to disordered flow termed resonant collapse by McEwan (1970) in the problem of forced inertial oscillations driven by rotating the top end of the cylinder at a given frequency (see also Kerswell 1999). Kobine (1995) attempted to determine the validity of the inviscid approximations via an experimental study, and found evidence of strong viscous boundary-layer phenomena when the conditions of resonance were approached. In addition to the theoretical analysis in their study, Meunier *et al.* (2008) also showed that the weakly nonlinear theory at resonance is in good agreement with the experimental result for weak precession.

There exist three characteristically different regimes in weakly precessing cylinders: (i) the regimes obeying the asymptotic scaling $|\boldsymbol{u}| = O(Po/\sqrt{Ek})$ for $Ek \ll 1$ at the primary resonances; (ii) the non-resonant regimes characterized by the asymptotic scaling $|\boldsymbol{u}| = O(Po)$ far away from the primary resonances; and (iii) the transition regimes from the resonant response with $|\boldsymbol{u}| = O(Po/\sqrt{Ek})$ to the non-resonant response with $|\boldsymbol{u}| = O(Po)$. In the transition regimes, both the interior and boundary-layer viscous effects become significant and a subset of the inertial modes are coupled by the viscous boundary-layer influx. Unlike at resonance (Gans 1970; Meunier *et al.* 2008), no particular asymptotic scalings are available in the transition regimes for simplifying the mathematical analysis, representing the most complicated regimes of the precession problem. It will be seen, moreover, that our analysis indicates that the classical inviscid approximation is always divergent even far away from the primary resonances and, hence, has limited physical and mathematical significance. There is a need to derive a general asymptotic solution that is valid at or near or away from the primary resonances and to determine the validity of both inviscid and viscous approximations by careful numerical experiments.

In what follows we shall begin by presenting the mathematical formulation of the problem in § 2. The divergent feature of an inviscid approximation and the derivation of a new general asymptotic solution are presented in § 3. Numerical analysis and its comparison with the general asymptotic solution are discussed in § 4 along with a brief summary.

2. Mathematical formulation

Consider a homogeneous fluid of viscosity ν confined in a fluid-filled circular cylinder of radius Γd and height d with volume $V = \pi(\Gamma d)^2 d$. As depicted in figure 1, the cylinder rotates rapidly with angular velocity $\boldsymbol{\Omega}_0 = \hat{\boldsymbol{z}}\Omega_0$ about its symmetry axis $\hat{\boldsymbol{z}}$, and precesses slowly with angular velocity $\boldsymbol{\Omega}_p$ that is fixed in space and at an angle α, $0 < \alpha \leqslant \pi/2$, with $\hat{\boldsymbol{z}}$. We shall adopt cylindrical polar coordinates (s, ϕ, z), with $s = 0$ representing the symmetry axis and $z = 0$ at the bottom surface,

https://doi.org/10.1017/jfm.2012.355 Published online by Cambridge University Press

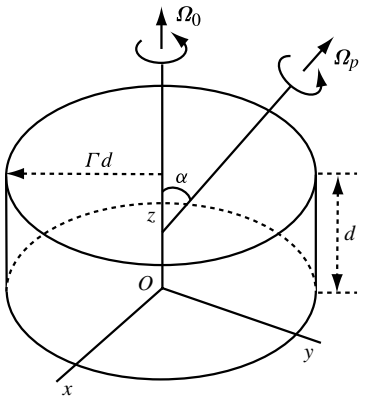


FIGURE 1. Geometry of a precessing right-circular cylinder with height d and radius–height aspect ratio Γ. Cartesian coordinates (x, y, z), or the corresponding cylindrical polar coordinates (s, ϕ, z), fixed in the cylinder will be adopted.

and the corresponding unit vectors $(\hat{\boldsymbol{s}}, \hat{\boldsymbol{\phi}}, \hat{\boldsymbol{z}})$. In these coordinates fixed in the container (Tilgner & Busse 2001), the body frame of reference, the precession vector $\boldsymbol{\Omega}_p$ is time-dependent,

$$\boldsymbol{\Omega}_p = |\boldsymbol{\Omega}_p|[\hat{\boldsymbol{s}} \sin\alpha \cos(\phi + \Omega_0 t) - \hat{\boldsymbol{\phi}} \sin\alpha \sin(\phi + \Omega_0 t) + \hat{\boldsymbol{z}} \cos\alpha], \tag{2.1}$$

and fluid motion driven by precession is described by the equations

$$\begin{aligned} &\frac{\partial \boldsymbol{u}}{\partial t} + \boldsymbol{u} \cdot \boldsymbol{\nabla} \boldsymbol{u} + 2\{\hat{\boldsymbol{z}}\Omega_0 + |\boldsymbol{\Omega}_p|[\hat{\boldsymbol{s}} \sin\alpha \cos(\phi + \Omega_0 t) \\ &\qquad - \hat{\boldsymbol{\phi}} \sin\alpha \sin(\phi + \Omega_0 t) + \hat{\boldsymbol{z}} \cos\alpha]\} \times \boldsymbol{u} \\ &\quad = -\boldsymbol{\nabla} p + \nu \nabla^2 \boldsymbol{u} - 2\hat{\boldsymbol{z}} |\boldsymbol{\Omega}_p| \Omega_0 s \sin\alpha \cos(\phi + \Omega_0 t)\,, \end{aligned} \tag{2.2}$$

$$\boldsymbol{\nabla} \cdot \boldsymbol{u} = 0, \tag{2.3}$$

where $\boldsymbol{u}$ is the velocity of fluid motion and p is the reduced pressure including the term $-sz|\boldsymbol{\Omega}_p|\Omega_0 \sin\alpha \cos(\phi + \Omega_0 t)$ resulting from the Poincaré force. The last term on the right-hand side of the equation of motion is known as the Poincaré forcing, which drives precessional flows against viscous dissipation.

Since there exist two angular velocities $\boldsymbol{\Omega}_0$ and $\boldsymbol{\Omega}_p$ in the precession system, various units of time have been adopted by different workers in scaling the equations (Wood 1966; Manasseh 1992; Kobine 1995; Meunier *et al.* 2008). We shall follow Tilgner & Busse (2001) in adopting Ω_0^{-1} as the time scale. On employing the height d as the length scale, Ω_0^{-1} as the unit of time and $\rho_0 d^2 \Omega_0^2$ as the unit of pressure, we obtain the dimensionless equations

$$\begin{aligned} &\frac{\partial \boldsymbol{u}}{\partial t} + \boldsymbol{u} \cdot \boldsymbol{\nabla} \boldsymbol{u} + 2\{\hat{\boldsymbol{z}} + Po[\hat{\boldsymbol{s}} \sin\alpha \cos(\phi + t) - \hat{\boldsymbol{\phi}} \sin\alpha \sin(\phi + t) + \hat{\boldsymbol{z}} \cos\alpha]\} \times \boldsymbol{u} \\ &\quad = -\boldsymbol{\nabla} p + Ek \nabla^2 \boldsymbol{u} - 2\hat{\boldsymbol{z}} s Po \sin\alpha \cos(\phi + t)\,, \end{aligned} \tag{2.4}$$

$$\boldsymbol{\nabla} \cdot \boldsymbol{u} = 0. \tag{2.5}$$

In the body frame of reference, the flow on the bounding surface $\mathscr{S}$ of a precessing circular cylinder is at rest, imposing

$$\hat{\boldsymbol{z}} \cdot \boldsymbol{u} = 0 \quad \text{and} \quad \hat{\boldsymbol{z}} \times \boldsymbol{u} = \boldsymbol{0} \tag{2.6}$$

https://doi.org/10.1017/jfm.2012.355 Published online by Cambridge University Press

on the bottom at $z=0$ and the top at $z=1$, and

$$\hat{\boldsymbol{s}}\cdot\boldsymbol{u}=0 \quad \text{and} \quad \hat{\boldsymbol{s}}\times\boldsymbol{u}=\boldsymbol{0} \tag{2.7}$$

on the sidewall at $s=\Gamma$.

When Po is sufficiently small ($Po\ll 1$) with the amplitude $|\boldsymbol{u}|=\epsilon\ll 1$, (2.4) may be linearized by omitting the higher-order terms, $\boldsymbol{u}\cdot\nabla\boldsymbol{u}=O(\epsilon^2)$ and

$$|Po[\hat{\boldsymbol{z}}\cos\alpha+\hat{\boldsymbol{s}}\sin\alpha\cos(\phi+t)-\hat{\boldsymbol{\phi}}\sin\alpha\sin(\phi+t)]\times\boldsymbol{u}|=O(Po\epsilon), \tag{2.8}$$

which results in the governing equations for a weakly precessing flow

$$\frac{\partial\boldsymbol{u}}{\partial t}+2\hat{\boldsymbol{z}}\times\boldsymbol{u}+\nabla p=Ek\nabla^2\boldsymbol{u}-2\hat{\boldsymbol{z}}sPo\sin\alpha\,\mathrm{e}^{\mathrm{i}(\phi+t)}, \tag{2.9}$$

$$\nabla\cdot\boldsymbol{u}=0, \tag{2.10}$$

where only the real part of the complex solution will be taken as the physical solution of the problem. It should be noted that, for small precession rate $Po\ll 1$, the angle α does not play a key role in the problem (Gans 1970).

The weakly precessing problem defined by (2.9)–(2.10) subject to the boundary conditions (2.6)–(2.7) will be first solved by an asymptotic method for $Ek\ll 1$ and then solved by a numerical method to check the validity and accuracy of the asymptotic solution.

3. Divergence of the inviscid solution and the general asymptotic solution

By assuming that the inviscid inertial modes are complete, any profile of the velocity $\boldsymbol{u}$ and pressure p in a precessing cylinder in the inviscid limit $Ek=0$ satisfying the inviscid boundary condition can be expanded in the form

$$\boldsymbol{u}=\left[\sum_{n=1}^{N}\sum_{k=1}^{2K}\mathscr{A}_{1nk}\boldsymbol{u}_{1nk}(s,\phi,z)\right]\mathrm{e}^{\mathrm{i}t},\quad p=\left[\sum_{n=1}^{N}\sum_{k=1}^{2K}\mathscr{A}_{1nk}p_{1nk}(s,\phi,z)\right]\mathrm{e}^{\mathrm{i}t}, \tag{3.1}$$

where triple index notion is adopted (the first index for the azimuthal wavenumber m of an inertial mode which is set to be $m=1$ because of the structure of the Poincaré force in (2.9), the axial wavenumber n and the radial wavenumber k), $\mathscr{A}_{1nk}$ are the unknown complex coefficients to be determined and the inertial modes $(\boldsymbol{u}_{1nk},p_{1nk})$ (Kelvin 1880; Greenspan 1968; Zhang & Liao 2008) are represented by

$$\hat{\boldsymbol{s}}\cdot\boldsymbol{u}_{1nk}(s,\phi,z)=\left[\frac{\sigma_{1nk}\xi_{1nk}}{\Gamma}\mathrm{J}_0\left(\frac{\xi_{1nk}s}{\Gamma}\right)+\frac{(1-\sigma_{1nk})}{s}\mathrm{J}_1\left(\frac{\xi_{1nk}s}{\Gamma}\right)\right]\times\left[\frac{-\mathrm{i}}{2(1-\sigma_{1nk}^2)}\right]\cos(n\pi z)\,\mathrm{e}^{\mathrm{i}\phi}, \tag{3.2}$$

$$\hat{\boldsymbol{\phi}}\cdot\boldsymbol{u}_{1nk}(s,\phi,z)=\left[\frac{\xi_{1nk}}{\Gamma}\mathrm{J}_0\left(\frac{\xi_{1nk}s}{\Gamma}\right)-\frac{(1-\sigma_{1nk})}{s}\mathrm{J}_1\left(\frac{\xi_{1nk}s}{\Gamma}\right)\right]\times\left[\frac{1}{2(1-\sigma_{1nk}^2)}\right]\cos(n\pi z)\,\mathrm{e}^{\mathrm{i}\phi}, \tag{3.3}$$

$$\hat{\boldsymbol{z}}\cdot\boldsymbol{u}_{1nk}(s,\phi,z)=\frac{-\mathrm{i}n\pi}{2\sigma_{1nk}}\left[\mathrm{J}_1\left(\frac{\xi_{mnk}s}{\Gamma}\right)\right]\sin n\pi z\mathrm{e}^{\mathrm{i}\phi}, \tag{3.4}$$

$$p_{1nk}(s,\phi,z)=\mathrm{J}_1\left(\frac{\xi_{1nk}s}{\Gamma}\right)\cos(n\pi z)\,\mathrm{e}^{\mathrm{i}\phi}. \tag{3.5}$$

https://doi.org/10.1017/jfm.2012.355 Published online by Cambridge University Press

In the above expressions, the radial wavenumber ξ_{1nk} is a solution of the transcendental equation,

$$\xi_{1nk}\mathrm{J}_0(\xi_{1nk}) + \left\{ \frac{\sigma_{1nk}}{|\sigma_{1nk}|}\left[1+\left(\frac{\xi_{1nk}}{\Gamma n\pi}\right)^2\right]^{1/2} - 1 \right\} \mathrm{J}_1(\xi_{1nk}) = 0, \tag{3.6}$$

while the half-frequency σ_{1nk} $(0 < |\sigma_{1nk}| < 1)$ of an inertial mode (i.e. the frequency $\omega_{1nk} = 2\sigma_{1nk}$) is computed from

$$\sigma_{1nk} = S_{pm}\left[1+\left(\frac{\xi_{1nk}}{\Gamma n\pi}\right)^2\right]^{-1/2}, \tag{3.7}$$

where $S_{pm} = \sigma_{1nk}/|\sigma_{1nk}|$. We shall label the radial wavenumber in ascending order $0 < \xi_{1n1} < \xi_{1n2} < \cdots < \xi_{1nk}, \ldots,$ with the corresponding half-frequency σ_{1nk} arranged as $1 > |\sigma_{1n1}| > |\sigma_{1n2}| > \cdots | > \sigma_{1nk}| \cdots > 0$. It is worth mentioning that $2K$ in the expansion (3.1) means that there are K lowest prograde modes ($\sigma_{1nk} < 0$) as well as K lowest retrograde modes ($\sigma_{1nk} > 0$) included in the expansion. With a straightforward analysis, one can show that $\mathscr{A}_{1nk}$ in the expansion (3.1) is

$$\mathscr{A}_{1nk} = \frac{-8Po\sin\alpha\Gamma^3[1-(-1)^n]\,(1+\sigma_{1nk})^2(1-\sigma_{1nk})}{\xi_{1nk}^2\left[(n\pi\Gamma)^2+(1-\sigma_{1nk})\right](1-2\sigma_{1nk})\,\mathrm{J}_1(\xi_{1nk})}, \tag{3.8}$$

with the kinetic energy density of a precessing flow, defined as $E_{kin} = 1/(2V)\int_V |\boldsymbol{u}|^2\,\mathrm{d}V$, given by

$$E_{kin} = \frac{1}{16\Gamma^2}\sum_{n=1}^{N}\sum_{k=1}^{2K}\left[\frac{(n\pi\Gamma)^2+(1-\sigma_{1nk})}{\sigma_{1nk}^2(1-\sigma_{1nk}^2)}\right]|\mathscr{A}_{1nk}|^2\,\mathrm{J}_1^2(\xi_{1nk}), \tag{3.9}$$

which provides a measure of the amplitude of the flow.

In addition to the weak discontinuity of the velocity across characteristics discussed by Wood (1966), our extensive calculation suggests that the inviscid approximation (3.1) is always divergent even away from resonances: both the flow structure and its amplitude depend sensitively on the truncation parameters N and K. Let us take the case $\Gamma = 1.3$ – which is far away from the primary resonances at $\Gamma = 1.045945$ and $\Gamma = 1.611089$ – to illustrate the main features of divergence. In any practical application, the expansion (3.1) must be truncated at certain levels of N and K. An approximation would be physically meaningful and useful if the expansion converged with increasing size of N and K. On the contrary, our calculation reveals that the inviscid solution (3.1) – its structure and amplitude – changes discontinuously at $(N = 3, K = 7)$, then at $(N = 7, K = 16)$ and then at $(N = 11, K = 25)$. These discontinuous changes, signalling the divergence of the expansion (3.1), would persist when further increasing N and K.

This divergent nature can be explained by the two resonant conditions discussed by Gans (1970):

$$\xi_{1nk}\mathrm{J}_0(\xi_{1nk}) + \mathrm{J}_1(\xi_{1nk}) = 0, \tag{3.10}$$

$$\sqrt{3}n\pi\Gamma - \xi_{1nk} = 0, \tag{3.11}$$

https://doi.org/10.1017/jfm.2012.355 Published online by Cambridge University Press

that must be satisfied in order that an inertial mode $\boldsymbol{u}_{1nk}$ resonates with the precessional forcing. It is well known (for example, Wood 1966; Meunier *et al.* 2008) that, at any given aspect ratio Γ, there exists an infinite number of higher-order inertial modes that approximately satisfy (3.10) and (3.11) and that can thus be arbitrarily close to the resonant conditions marked by odd n and $\sigma_{1nk} = 1/2$. At the fixed aspect ratio $\Gamma = 1.3$, for example, (3.10) and (3.11) are approximately satisfied when $n = 3$ and $k = 7$ (the radial wavenumber $\xi_{1nk} = 21.2587$) with $\sigma_{1nk} = 0.49934$; they are approximately satisfied for $n = 7$ and $k = 16$ (the radial wavenumber $\xi_{1nk} = 49.5028$) with $\sigma_{1nk} = 0.50010$; and $n = 11$ and $k = 25$ (the radial wavenumber $\xi_{1nk} = 77.7689$) with $\sigma_{1nk} = 0.50010$ also represent an approximate solution to (3.10) and (3.11). In consequence, the singularity in the expression (3.8) cannot be removed by moving the key parameters away from the primary resonances. The existence of discontinuous variations with increasing N and K suggests that the inviscid approximation (3.1) cannot compare quantitatively with the experimental observation or with the numerical solution, even away from resonances.

In order to derive a general asymptotic solution at $Ek \ll 1$ that is convergent and valid at or near or away from the primary resonances, we must include small viscous effects previously neglected, and modify the inviscid expansion (3.1) to have the form

$$\boldsymbol{u}(s,\phi,z,t) = \left[\left(\sum_{n=1}^{N}\sum_{k=1}^{2K} \mathscr{A}_{1nk}\boldsymbol{u}_{1nk}\right) + \widehat{\boldsymbol{u}} + \widetilde{\boldsymbol{u}}\right] \mathrm{e}^{\mathrm{i}t}, \tag{3.12}$$

$$p(s,\phi,z,t) = \left[\left(\sum_{n=1}^{N}\sum_{k=1}^{2K} \mathscr{A}_{1nk}p_{1nk}\right) + \widehat{p} + \widetilde{p}\right] \mathrm{e}^{\mathrm{i}t}, \tag{3.13}$$

where $\widehat{\boldsymbol{u}}$ and $\widehat{p}$ represent small interior perturbations, caused by both the interior viscous effect and the viscous boundary layer $\widetilde{\boldsymbol{u}}$ and $\widetilde{p}$, with $|\widehat{\boldsymbol{u}}| \ll |\mathscr{A}_{1nk}\boldsymbol{u}_{1nk}|$ but $|\widetilde{\boldsymbol{u}}| = O|\sum_{n,k}\mathscr{A}_{1nk}\boldsymbol{u}_{1nk}|$. Since the effect of viscous boundary layers couples a subset of the inertial modes together, the mathematical analysis of the general asymptotic solution becomes much more complicated and a simple analytical solution is no longer feasible.

On introducing the viscous effect in both the interior and boundary layers, the coefficients $\mathscr{A}_{1nk}$ in the modified expansion (3.12) and (3.13) are determined by a system of the coupled equations,

$$\left[\mathrm{i}(1-2\sigma_{1nk}) + \frac{Ek\,(n\pi)^2}{\sigma_{1nk}^2}\right]\mathscr{A}_{1nk}\int_0^1\int_0^{\Gamma}\int_0^{2\pi} |\boldsymbol{u}_{1nk}|^2 s\,\mathrm{d}\phi\,\mathrm{d}s\,\mathrm{d}z + \int_{\mathscr{S}} p_{1nk}^*\left(\hat{\boldsymbol{n}}\cdot\widehat{\boldsymbol{u}}\right)\mathrm{d}\mathscr{S} = -2Po\sin\alpha\int_0^1\int_0^{\Gamma}\int_0^{2\pi}\hat{\boldsymbol{z}}\cdot\boldsymbol{u}_{1nk}^* s^2\,\mathrm{d}\phi\,\mathrm{d}s\,\mathrm{d}z \tag{3.14}$$

for $n = 1, 2, 3, \ldots,$ and $k = 1, 2, 3, \ldots,$ where f^* denotes the complex conjugate of f and $\int_{\mathscr{S}}\mathrm{d}\mathscr{S}$ represents an integral over the bounding surface $\mathscr{S}$ of the cylinder. There exist three viscous boundary layers – $\widetilde{\boldsymbol{u}}_{top}$ on the top ($z = 1$), $\widetilde{\boldsymbol{u}}_{bottom}$ on the bottom ($z = 0$) and $\widetilde{\boldsymbol{u}}_{sidewall}$ at the sidewall ($s = \Gamma$) – in a precessing cylinder at $Ek \ll 1$. It is the surface integral $\int_{\mathscr{S}} p_{1nk}^*(\hat{\boldsymbol{n}}\cdot\widehat{\boldsymbol{u}})\,\mathrm{d}\mathscr{S}$ that links the boundary-layer flow $\widetilde{\boldsymbol{u}}$ with the mainstream, and that is usually involved in lengthy mathematical analysis (for example, Zhang & Liao 2009). After some manipulation, the system (3.14) can be

https://doi.org/10.1017/jfm.2012.355 Published online by Cambridge University Press

written in terms of the three viscous boundary layers:

$$\left[\mathrm{i}(1-2\sigma_{1nk})+\frac{Ek\,(n\pi)^2}{\sigma_{1nk}^2}\right]\mathscr{A}_{1nk}\int_0^1\int_0^\Gamma\int_0^{2\pi}|\boldsymbol{u}_{1nk}|^2 s\,\mathrm{d}\phi\,\mathrm{d}s\,\mathrm{d}z$$
$$-\sqrt{Ek}\int_0^1\int_0^{2\pi}\left(2\mathrm{i}\sigma_{1nk}\boldsymbol{u}_{1nk}^*-2\hat{\boldsymbol{z}}\times\boldsymbol{u}_{1nk}^*\right)_{s=\Gamma}\cdot\left(\int_0^\infty\widetilde{\boldsymbol{u}}_{sidewall}\,\mathrm{d}\eta_s\right)\Gamma\,\mathrm{d}\phi\,\mathrm{d}z$$
$$-2\sqrt{Ek}\int_0^\Gamma\int_0^{2\pi}\left(2\mathrm{i}\sigma_{1nk}\boldsymbol{u}_{1nk}^*-2\hat{\boldsymbol{z}}\times\boldsymbol{u}_{1nk}^*\right)_{z=0}\cdot\left(\int_0^\infty\widetilde{\boldsymbol{u}}_{bottom}\,\mathrm{d}\eta_0\right)s\,\mathrm{d}\phi\,\mathrm{d}s$$
$$=-2Po\sin\alpha\int_0^1\int_0^\Gamma\int_0^{2\pi}\hat{\boldsymbol{z}}\cdot\boldsymbol{u}_{1nk}^*s^2\,\mathrm{d}\phi\,\mathrm{d}s\,\mathrm{d}z,\tag{3.15}$$

where $\eta_0=z/\sqrt{Ek}$, a stretched boundary-layer variable, for the bottom boundary layer $\widetilde{\boldsymbol{u}}_{bottom}$ while $\eta_s=(\Gamma-s)/\sqrt{Ek}$ for the sidewall boundary layer $\widetilde{\boldsymbol{u}}_{sidewall}$. Note that the symmetry properties between $\widetilde{\boldsymbol{u}}_{bottom}$ and $\widetilde{\boldsymbol{u}}_{top}$ introduce a factor 2 in the third term of the left-hand side.

After obtaining the viscous boundary layers $\widetilde{\boldsymbol{u}}_{bottom}$ and $\widetilde{\boldsymbol{u}}_{sidewall}$, which are given by

$$\widetilde{\boldsymbol{u}}_{bottom}=-\frac{1}{2}\sum_{n=1}^{N}\sum_{k=1}^{2K}\mathscr{A}_{1nk}\left\{\left(\boldsymbol{u}_{1nk}-\mathrm{i}\hat{\boldsymbol{z}}\times\boldsymbol{u}_{1nk}\right)_{z=0}\mathrm{e}^{-\sqrt{6}(1+\mathrm{i})\eta_0/2}\right.$$
$$\left.+\left(\boldsymbol{u}_{1nk}+\mathrm{i}\hat{\boldsymbol{z}}\times\boldsymbol{u}_{1nk}\right)_{z=0}\mathrm{e}^{-\sqrt{2}(1-\mathrm{i})\eta_0/2}\right\},\tag{3.16}$$

$$\widetilde{\boldsymbol{u}}_{sidewall}=-\sum_{n=1}^{N}\sum_{k=1}^{2K}\left[\mathscr{A}_{1nk}(\boldsymbol{u}_{1nk})_{s=\Gamma}\right]\mathrm{e}^{-\sqrt{2}\eta_s(1+\mathrm{i})/2},\tag{3.17}$$

and carrying out the relevant integrations, we obtain that

$$\left[\mathrm{i}(1-2\sigma_{1nk})+\frac{Ek\,(n\pi)^2}{\sigma_{1nk}^2}\right]\left\{\frac{\left[(n\pi\Gamma)^2+(1-\sigma_{1nk})\right]\mathrm{J}_1^2(\xi_{1nk})}{4\sigma_{1nk}^2(1-\sigma_{1nk}^2)}\right\}\mathscr{A}_{1nk}$$
$$+\frac{\sqrt{Ek}\sqrt{2}\Gamma(1+\mathrm{i})\mathrm{J}_1(\xi_{1nk})}{4}\left[(n\pi)^2+\frac{1}{\Gamma^2}\right]\sum_{k'=1}^{2K}\left[\frac{\mathrm{J}_1(\xi_{1nk'})}{\sigma_{1nk'}}\right]\mathscr{A}_{1nk'}$$
$$+\frac{\sqrt{Ek}\sqrt{6}}{3}\left\{\left[1+\sqrt{3}+(1-\sqrt{3})\sigma_{1nk}+\mathrm{i}\left(1-\sqrt{3}+(1+\sqrt{3})\sigma_{1nk}\right)\right]\right.$$
$$\times\sum_{n'=1}^{N}\sum_{k'=1}^{2K}\left[\int_0^\Gamma\left(\boldsymbol{u}_{1nk}^*\cdot\boldsymbol{u}_{1n'k'}\right)_{z=0}s\,\mathrm{d}s\right]\mathscr{A}_{1n'k'}$$
$$+\left[1+\sqrt{3}+(1-\sqrt{3})\sigma_{1nk}-\mathrm{i}\left(1-\sqrt{3}+(1+\sqrt{3})\sigma_{1nk}\right)\right]$$
$$\left.\times\sum_{n'=1}^{N}\sum_{k'=1}^{2K}\left[\int_0^\Gamma\hat{\boldsymbol{z}}\cdot\left(\boldsymbol{u}_{1n'k'}\times\boldsymbol{u}_{1nk}^*\right)_{z=0}s\,\mathrm{d}s\right]\mathscr{A}_{1n'k'}\right\}$$
$$=-2Po\sin\alpha\left\{\frac{\mathrm{i}\Gamma^3[1-(-1)^n](1+\sigma_{1nk})}{(\sigma_{1nk}\xi_{1nk})^2}\right\}\mathrm{J}_1(\xi_{1nk})\tag{3.18}$$

for $n=1,2,3,\ldots$ and $k=1,2,3,\ldots,$ representing a system of linear algebraic equations for $\mathscr{A}_{1nk}$ which can be readily solved. After solving the equation (3.18)

https://doi.org/10.1017/jfm.2012.355 Published online by Cambridge University Press

for $\mathscr{A}_{1nk}$, the leading-order solution for the precessing flow can be expressed as

$$\boldsymbol{u}(s,\phi,z,t)=\left[\left(\sum_{n=1}^{N}\sum_{k=1}^{2K}\mathscr{A}_{1nk}\boldsymbol{u}_{1nk}\right)+\widetilde{\boldsymbol{u}}_{bottom}+\widetilde{\boldsymbol{u}}_{top}+\widetilde{\boldsymbol{u}}_{sidewall}\right]\mathrm{e}^{\mathrm{i}t},\tag{3.19}$$

where $\boldsymbol{u}_{1nk}$ is given by (3.2)–(3.4), $\widetilde{\boldsymbol{u}}_{bottom}$ by (3.16), $\widetilde{\boldsymbol{u}}_{sidewall}$ by (3.17), and $\widetilde{\boldsymbol{u}}_{top}$ is given by

$$\begin{aligned}\widetilde{\boldsymbol{u}}_{top}=-\frac{1}{2}\sum_{n=1}^{N}\sum_{k=1}^{2K}\mathscr{A}_{1nk}\Big\{&\left(\boldsymbol{u}_{1nk}-\mathrm{i}\hat{\boldsymbol{z}}\times\boldsymbol{u}_{1nk}\right)_{z=1}\mathrm{e}^{-\sqrt{6}(1+\mathrm{i})\eta_1/2}\\&+\left(\boldsymbol{u}_{1nk}+\mathrm{i}\hat{\boldsymbol{z}}\times\boldsymbol{u}_{1nk}\right)_{z=1}\mathrm{e}^{-\sqrt{2}(1-\mathrm{i})\eta_1/2}\Big\}\end{aligned}\tag{3.20}$$

with $\eta_1=(1-z)/\sqrt{Ek}$. Its kinetic energy density, E_{kin}, at leading-order approximation, is

$$E_{kin}=\frac{1}{16\Gamma^2}\sum_{n=1}^{N}\sum_{k=1}^{2K}\left[\frac{(n\pi\Gamma)^2+(1-\sigma_{1nk})}{\sigma_{1nk}^2(1-\sigma_{1nk}^2)}\right]\left[|\mathscr{A}_{1nk}|\mathrm{J}_1(\xi_{1nk})\right]^2+O(\sqrt{Ek}).\tag{3.21}$$

The asymptotic solution given by (3.19) and (3.21) is convergent, valid at or near or away from the primary resonance for $Ek\ll 1$, satisfies the no-slip boundary condition and will be validated by the corresponding numerical analysis.

4. Numerical analysis: comparison between asymptotics and numerics

A non-axisymmetric velocity vector satisfying $\nabla\cdot\boldsymbol{u}=0$ in cylindrical geometry can be expressed in terms of two scalar potentials $\Psi(s,\phi,z)$ and $\Phi(s,\phi,z)$ (Marqués 1990):

$$\boldsymbol{u}=\left[\nabla\times\left(\hat{\boldsymbol{s}}\Psi\right)+\nabla\times\left(\hat{\boldsymbol{z}}\Phi\right)\right]\mathrm{e}^{\mathrm{i}t}=\left[\frac{1}{s}\frac{\partial\Psi}{\partial\phi}\hat{\boldsymbol{s}}+\left(\frac{\partial\Phi}{\partial z}-\frac{\partial\Psi}{\partial s}\right)\hat{\boldsymbol{\phi}}-\frac{1}{s}\frac{\partial\Phi}{\partial\phi}\hat{\boldsymbol{z}}\right]\mathrm{e}^{\mathrm{i}t}.\tag{4.1}$$

An important advantage in using (4.1) is that the two scalar potentials are decoupled for the velocity boundary condition on the stress-free or no-slip sidewall. In terms of Ψ and Φ, the non-slip velocity condition on the sidewall is imposed by

$$\Psi=\frac{\partial\Psi}{\partial s}=\Phi=0\quad\text{at } s=\Gamma,\tag{4.2}$$

$$\Psi=\frac{\partial\Phi}{\partial z}=\Phi=0\quad\text{at } z=0,1.\tag{4.3}$$

Making use of the expression (4.1) and applying $\hat{\boldsymbol{z}}\cdot\nabla\times$ and $\hat{\boldsymbol{s}}\cdot\nabla\times$ onto (2.9), we can derive the two independent scalar equations,

$$\left(\mathrm{i}-Ek\nabla^2\right)\left[\frac{1}{s}\frac{\partial}{\partial s}\left(s\frac{\partial\Phi}{\partial z}\right)-\left(\nabla^2-\frac{\partial^2}{\partial z^2}\right)\Psi\right]+\frac{2}{s}\frac{\partial^2\Phi}{\partial z\partial\phi}=0,\tag{4.4}$$

$$\begin{aligned}&\left[\mathrm{i}-Ek\left(\nabla^2+\frac{2}{s}\frac{\partial}{\partial s}+\frac{1}{s^2}\right)\right]\left[\frac{\partial^2\Psi}{\partial s\partial z}-\left(\nabla^2-\frac{1}{s}\frac{\partial}{\partial s}s\frac{\partial}{\partial s}\right)\Phi\right]-\frac{2}{s}\frac{\partial^2\Psi}{\partial z\partial\phi}\\&\quad-\frac{2Ek}{s}\left[\frac{1}{s}\frac{\partial}{\partial s}\left(s\frac{\partial^2\Phi}{\partial z^2}\right)-\left(\nabla^2-\frac{\partial^2}{\partial z^2}\right)\frac{\partial\Psi}{\partial z}\right]=-2\mathrm{i}Po\sin\alpha\mathrm{e}^{\mathrm{i}\phi}.\end{aligned}\tag{4.5}$$

https://doi.org/10.1017/jfm.2012.355 Published online by Cambridge University Press

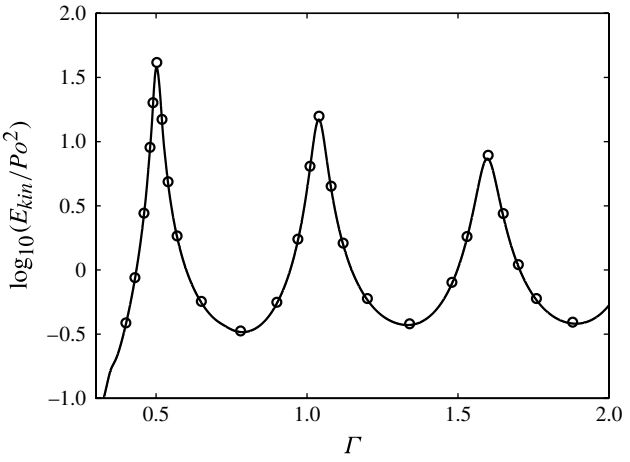


FIGURE 2. Scaled kinetic energies, E_{kin}/Po^2, of the precessing flow as a function of the aspect ratio Γ (the solid line) based on the numerical analysis, while the circles denote the results of the general asymptotic solution (3.21). The parameters are $Po = 10^{-4}$ and $Ek = 5 \times 10^{-5}$ with $\alpha = \pi/4$. The three peaks correspond to the three primary resonances at aspect ratios $\Gamma = 0.502559$ (resonating with the inertial mode $\boldsymbol{u}_{111}$), $\Gamma = 1.045945$ (resonating with the inertial mode $\boldsymbol{u}_{112}$) and $\Gamma = 1.611089$ (resonating with the inertial mode $\boldsymbol{u}_{113}$).

Equations (4.4) and (4.5) are then solved numerically by using the Galerkin method in which the potential fields Φ and Ψ are expanded in terms of the standard Chebyshev polynomials T_k,

$$\Psi = s\left(1 - \frac{s}{\Gamma}\right)^2 \left[1 - (2z-1)^2\right] \sum_{k=0}^{K} \sum_{n=0}^{N} \hat{\Psi}_{kn} T_k \left(\frac{2s}{\Gamma} - 1\right) T_n (2z-1)\, \mathrm{e}^{\mathrm{i}\phi}, \tag{4.6}$$

$$\Phi = s^2 \left(1 - \frac{s}{\Gamma}\right) \left[1 - (2z-1)^2\right]^2 \sum_{k=0}^{K} \sum_{n=0}^{N} \hat{\Phi}_{kn} T_k \left(\frac{2s}{\Gamma} - 1\right) T_n (2z-1)\, \mathrm{e}^{\mathrm{i}\phi}, \tag{4.7}$$

where $\hat{\Psi}_{kn}$, $\hat{\Phi}_{kn}$ are complex coefficients and the factors s and s^2 are imposed so that the expansion at the rotation axis $s = 0$ is regular. An application of the standard Galerkin procedure gives rise to a system of linear algebraic equations for $\hat{\Psi}_{kn}$ and $\hat{\Phi}_{kn}$ which can be readily solved by an iterative method. For numerical solutions with $Ek \geqslant O(10^{-5})$, we need to take $N = O(100)$ and $K = O(100)$ for accuracy within 1 %. Note that the no-slip boundary conditions on the bounding surface of the cylinder are automatically satisfied by the Galerkin expansion.

The primary purpose of the numerical analysis, which is valid for large or moderately small Ek, is to provide a valuable validation against the result of the asymptotic analysis valid only for $Ek \ll 1$. It is found that the general asymptotic solution (3.19) and (3.21) achieves good quantitative agreement with the fully numerical solution at or near or away from resonances, and correctly captures both the asymptotic scalings, $|\boldsymbol{u}| \sim Po/\sqrt{Ek}$ and $|\boldsymbol{u}| \sim Po$, and the transition between them. This agreement is clearly displayed in figure 2, which shows the scaled kinetic energies E_{kin}/Po^2, obtained from both the asymptotic expression (3.21) and the

https://doi.org/10.1017/jfm.2012.355 Published online by Cambridge University Press

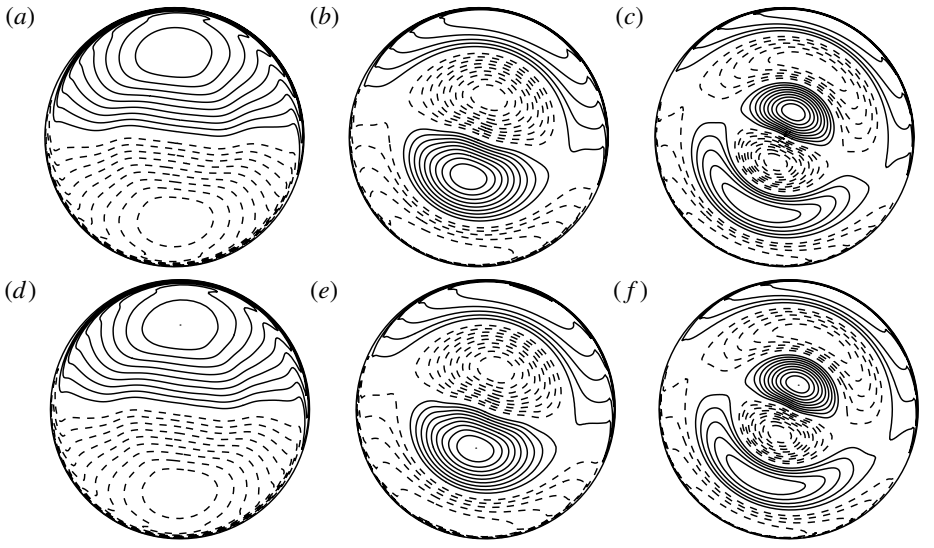


FIGURE 3. Contours of u_z at the $z = 1/2$ plane: (a–c) computed from the numerical solution, (d–f) obtained from the general asymptotic solution (3.19). All three solutions take $Po = 10^{-4}$, $\alpha = \pi/4$ with $E = 5 \times 10^{-5}$ but for different values of aspect ratio Γ: (a,d) $\Gamma = 0.502559$, (b,e) $\Gamma = 1.045945$, (c,f) $\Gamma = 1.611089$.

corresponding numerical solution, as a function of aspect ratio Γ for fixed $Po = 10^{-4}$ and $Ek = 5 \times 10^{-5}$ with $\alpha = 45^\circ$.

The spatial structures of the precessing flow at the three primary resonances $\Gamma = 0.502559$, $\Gamma = 1.045945$ and $\Gamma = 1.611089$, which correspond to the three peaks in figure 2, are depicted in figure 3, where (a–c) represents the numerical solution to (4.4) and (4.5) while (d–f) is obtained from the asymptotic expression (3.19). There exist no noticeable differences between the asymptotic and numerical solutions at the primary resonances. Away from the resonances, good quantitative agreement is also achieved. Figure 4 depicts the structures of the precessing flow for $Po = 10^{-4}$, $\alpha = \pi/4$ and $E = 5 \times 10^{-5}$ at $\Gamma = 1.3$, plotted from both the asymptotic expression (3.19) and the numerical solution of (4.4) and (4.5). Again there are no noticeable differences between the asymptotic and numerical solutions. Unlike the inviscid solution (3.1), whose pattern and amplitude change discontinuously with the truncation parameter K and N, the general asymptotic solutions for $Ek \ll 1$, displayed in figures 2–4, converge well, and remain nearly unchanged and independent of K and N after $K \geqslant 5$ and $N \geqslant 5$. The divergence of the inviscid approximation (3.1) in the non-resonant regimes is removed by the effect of weak viscosity in both the viscous boundary layer and the interior.

In summary, we have derived the first general asymptotic solution (3.19) and (3.21) that is valid at or near or away from the primary resonances and that correctly captures the key dynamics in the transition regime ranging from the direct resonance (which has the asymptotic scaling $|\boldsymbol{u}| = O(Po)/\sqrt{Ek}$) for $Ek \ll 1$) to the non-resonance (which has the asymptotic scaling $|\boldsymbol{u}| = O(Po)$ for $Ek \ll 1$) in weakly precessing cylinders. We have also provided a valuable validation between the general asymptotic solution and the numerical simulation, showing that excellent quantitative agreement is achieved between the asymptotic and the numerical analysis at or near or away from

https://doi.org/10.1017/jfm.2012.355 Published online by Cambridge University Press

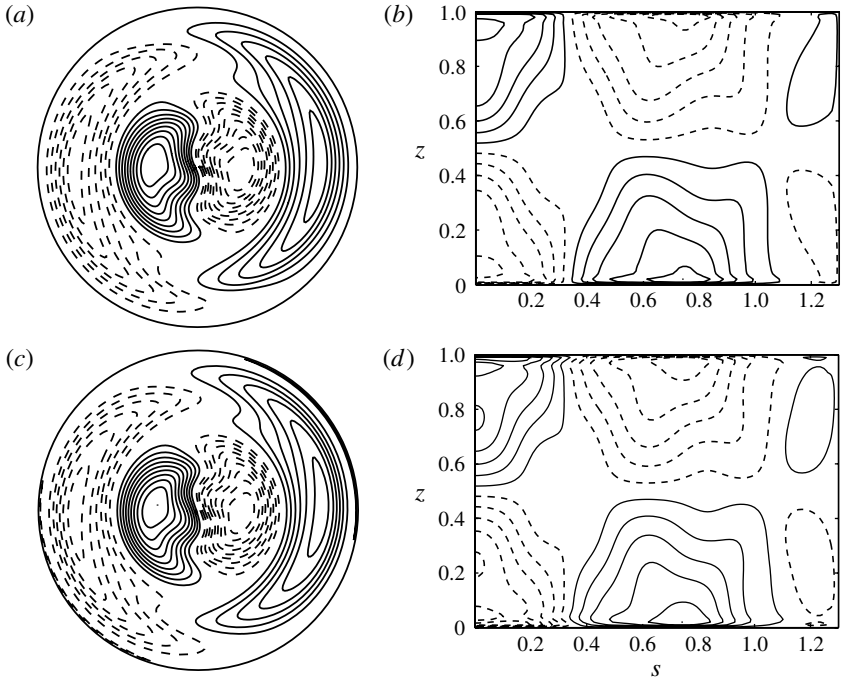


FIGURE 4. (*a*) Contours of u_z at the $z = 1/2$ plane; (*b*) contours of u_ϕ at the vertical plane $\phi = \pi/4$ computed from numerical analysis; (*c*) contours of u_z at the $z = 1/2$ plane; (*d*) contours of u_ϕ at the vertical plane $\phi = \pi/4$ from the general asymptotic solution (3.19). The parameters are $Po = 10^{-4}$, $\alpha = \pi/4$ and $E = 5 \times 10^{-5}$ at $\Gamma = 1.3$.

resonances. The general asymptotic solution found in this paper would be particularly useful for the understanding of experimental studies performed for parameters that are near or away from the primary resonances.

Acknowledgements

X.L. is supported by the NSFC under grant number 11133004 and the Chinese Academy of Sciences under grant number KZZD-EW-01-3. K.Z. is supported by UK Leverhulme, STFC and NERC grants. The numerical computation is supported by Shanghai Supercomputer Center.

REFERENCES

GANS, R. F. 1970 On the precession of a resonant cylinder. *J. Fluid Mech.* **41**, 865–872.

GREENSPAN, H. P. 1968 *The Theory of Rotating Fluids*. Cambridge University Press.

KELVIN, LORD 1880 Vibrations of a columnar vortex. *Phil. Mag.* **10**, 155–168.

KERSWELL, R. R. 1999 Secondary instabilities in rapidly rotating fluids: inertial wave breakdown. *J. Fluid Mech.* **382**, 283–306.

KOBINE, J. J. 1995 Inertial wave dynamics in a rotating and precessing cylinder. *J. Fluid Mech.* **303**, 233–252.

KOBINE, J. J. 1996 Azimuthal flow associated with inertial wave resonance in a precessing cylinder. *J. Fluid Mech.* **319**, 387–406.

https://doi.org/10.1017/jfm.2012.355 Published online by Cambridge University Press

MANASSEH, R. 1992 Breakdown regimes of inertia waves in a precessing cylinder. *J. Fluid Mech.* **243**, 261–296.

MARQUÉS, F. 1990 On boundary conditions for velocity potentials in confined flows: application to Couette flow. *Phys. Fluids* A **2**, 729–737.

MCEWAN, A. D 1970 Inertial oscillations in a rotating fluid cylinder. *J. Fluid Mech.* **40**, 603–640.

MEUNIER, P., ELOY, C., LAGRANGE, R. & NADAL, F. 2008 A rotating fluid cylinder subject to weak precession. *J. Fluid Mech.* **599**, 405–440.

TILGNER, A. & BUSSE, F. H. 2001 Fluid flows in precessing spherical shells. *J. Fluid Mech.* **426**, 387–396.

WOOD, W. W. 1966 An oscillatory disturbance of rigidly rotating fluid. *Proc. R. Soc. Lond.* A **293**, 181–212.

WU, C. C. & ROBERTS, P. H. 2009 On a dynamo driven by topographic precession. *Geophys. Astrophys. Fluid Dyn.* **103**, 467–501.

ZHANG, K. & LIAO, X. 2008 On the initial value problem in a rotating circular cylinder. *J. Fluid Mech.* **610**, 425–443.

ZHANG, K. & LIAO, X. 2009 The onset of convection in rotating circular cylinders with experimental boundary conditions. *J. Fluid Mech.* **622**, 63–73.

https://doi.org/10.1017/jfm.2012.355 Published online by Cambridge University Press